Electronic Supplementary Material (ESI) for RSC Advances

SUPPLEMENARY INFORMATION (SI)

The nature of synthetic Basic Ferric Arsenate Sulfate ($Fe(AsO_4)_{1-x}(SO_4)_x(OH)_x$) and Basic Ferric Sulfate ($FeOHSO_4$): Their crystallographic, molecular and electronic structure with applications in the environment and energy fields (Supplementary Information)

M. A. Gomez[a]*, G. Ventruti[b], M. Celikin[a], H. Assaaoudi[a], H. Putz[c], L. Becze[a], K.E. Lee[a] and G. P. Demopoulos[a]*

[a] Dr. M. A. Gomez, Dr. H. Assaaoudi, Dr. Mert Celikin, Dr. L. Becze, Dr. K.E. Lee and Prof G. P. Demopoulos
Materials Engineering
McGill University
3610 University Street, Montreal, Canada
Fax: 1- 514-398-4492
E-mail:mario.gomez@mail.mcgill.ca and george.demopoulos@mcgill.ca

[b] Dr. G. Ventruti
Dipartimento di Scienze della Terra e Geoambientali
Università di Bari Aldo Moro
Via Orabona, 4, 70125 Bari, Italy

[c] Dr. H. Putz
Crystal Impact
Bonn, Germany, D-53111

Section 1 : Supplementary Experimental information

Detailed Experimental Section

Synthesis

For the synthesis of these phases, analytical-reagent grade $As_2O_5 \cdot xH_2O$ and $Fe_2(SO_4)_3 \cdot xH_2O$ were dissolved in water in the desired molar proportions (C_{Fe} = 0.30 - 0.40 M and C_{As} = 0.09 - 0.40 M) to give different starting Fe(III) to As(V) molar ratios. The resulting solutions were left at their natural pH (≤ 1) and were placed in a two liter Parr titanium autoclave and heated to the desired temperature (175 - 225 °C) and held there for the desired reaction time. The resulting slurries were then filtered after cooling using a pressure filter and a 0.1 μm filter paper. Following thorough washing, the solids were subjected to characterization Additional experimental details and elemental compositions maybe found in previous published work.[14] The experimental synthesis conditions and solid composition (determined via ICP-OES) of the phases investigated in this study are presented in Table 1. The formation of these iron (III) arsenate-sulfate phases such as the BFAS can be described by the following general reaction[14]:

$$Fe(SO_4)_{1.5} + H_3AsO_4 + (w+z/2)H_2O \rightarrow Fe(AsO_4)_x(SO_4)_y(OH)_z \cdot wH_2O + (1.5-y)H_2SO_4$$

Scheme 1. Formation of the arsenate and sulfate rich BFAS and arsenate containing BFS phases

Powder X-ray Diffraction (Lab and Synchrotron based)

The lab based PXRD analysis was performed with a RigakuRotaflex D-Max diffractometer equipped with a rotation anode, a copper target (λ Cu K_α = 1.5046 Å), a monochromator composed of a graphite crystal and a scintillator detector. The diffractometer used 40 kV and 150 mA. The scans were recorded between 5 and 100° 2θ with a 0.1° step size and an acquisition time of three seconds per step.

High resolution synchrotron powder diffraction data for structural analysis was collected for BFS, and the two BFAS samples (arsenate and sulfate rich) using beamline 11-BM at the Advanced Photon Source (APS) using a wavelength of 0.4587(2) Å.[21] Discrete detectors covering an angular range from −6 to 16° 2θ are scanned over a 45° 2θ range; with data points collected every 0.001° 2θ and scan speed of 0.01° s^{-1}. Data are collected while continually scanning the diffractometer 2θ arm. A mixture of NIST standard reference materials, Si (SRM 640c) and Al_2O_3 (SRM 676) is used to calibrate the instrument, where the Si lattice constant determines the wavelength for each detector. Corrections are applied for detector sensitivity, 2θ offset, small differences in wavelength between detectors, and the source intensity, as noted by the ion chamber before merging the data into a single set of intensities evenly spaced in 2θ. Structures were first indexed with the Crysfire suite program then estimated with Endevour[22] and finally refined with the Rietveld method employed by the General Structure Analysis System (GSAS)[23-24] and DIFFaX[25].

SEM and TEM

The morphological characterization of the three phases was done on the Field Emission Gun Scanning Electron Microscope (FEG-SEM) Hitachi S-4700. Prior to the morphological analysis, the produced solids were deposited on carbon double sided tape and coated with a thin layer of AuPd. The TEM analysis was done with the use of the FEG-TEM JEOL** 2100F @ 200kV. This microscope was equipped with a scanning transmission electron microscopy (STEM) detector and an energy-dispersive spectrometer (EDS) detector. Particles were deposited on a Cu grid with an amorphous carbon film prior to their examination and observed to ensure no beam damage had occurred. The TEM instrument was equipped with a double-tilt holder (maximum angle change: 20° in two different rotation axis) used for the electron diffraction structure analysis. In order to obtain crystallographic information of a phase, the sample was tilted to certain zone axis using Kikuchi patterns as guidelines when the thickness was sufficient. Then, three SAED patterns were taken for a zone axis. Tilting was again conducted (where feasible) to obtain another zone axis where the tilting angle between each zone axis was recorded. The procedure was repeated until 2-4 single crystal SAED patterns and the angle between each were recorded for a phase. Moreover, to facilitate the analysis of the electron diffraction patterns and for final validation, the SAED patterns were also computed via the crystallography software (Carine Crystallography) using our crystallographic data obtained from the XRD analysis. First hematite was indexed for quality check of our camera constant before doing the BFAS (3185) phase. The indexed diffraction patterns agree well for

Hematite- trigonal hexagonal (a: 5.0293Å and c: 13.864 Å) and BFAS (3185) monoclinic (a: 7.5980, b: 7.3063, c: 7.5580 and β = 120.387°) structures. BFAS (3185) angles and r-ratios between diffraction spots (planes) for 2 zone axis [011] and [012]), the created reciprocal lattices of the SAED patterns obtained from TEM analysis are shown below.

Hematite

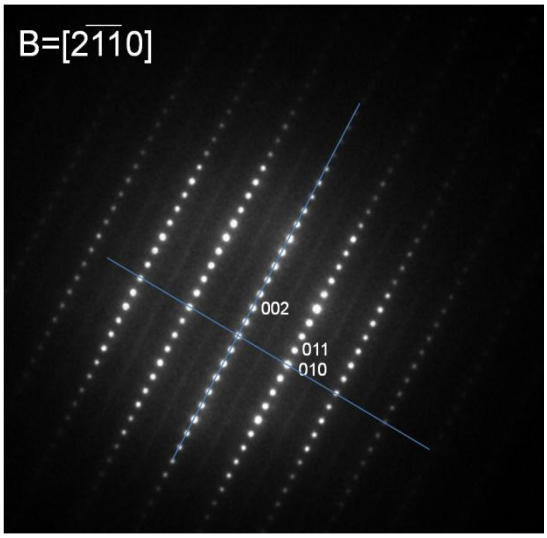

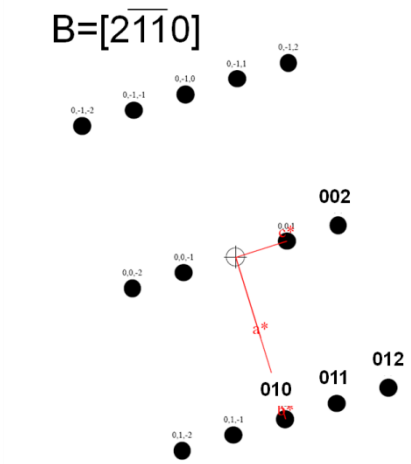

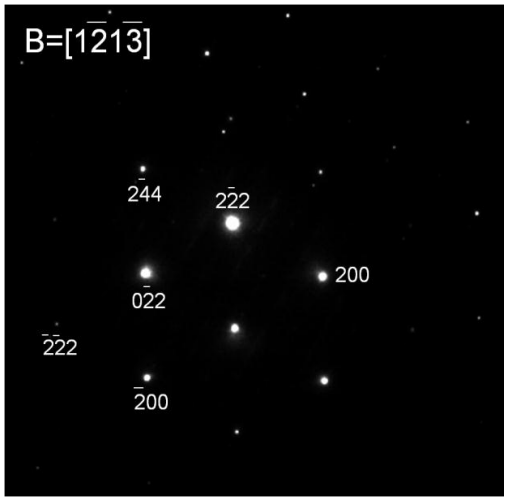

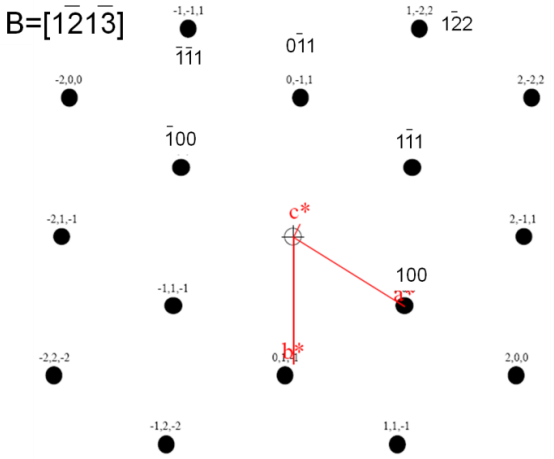

BFAS (3185)

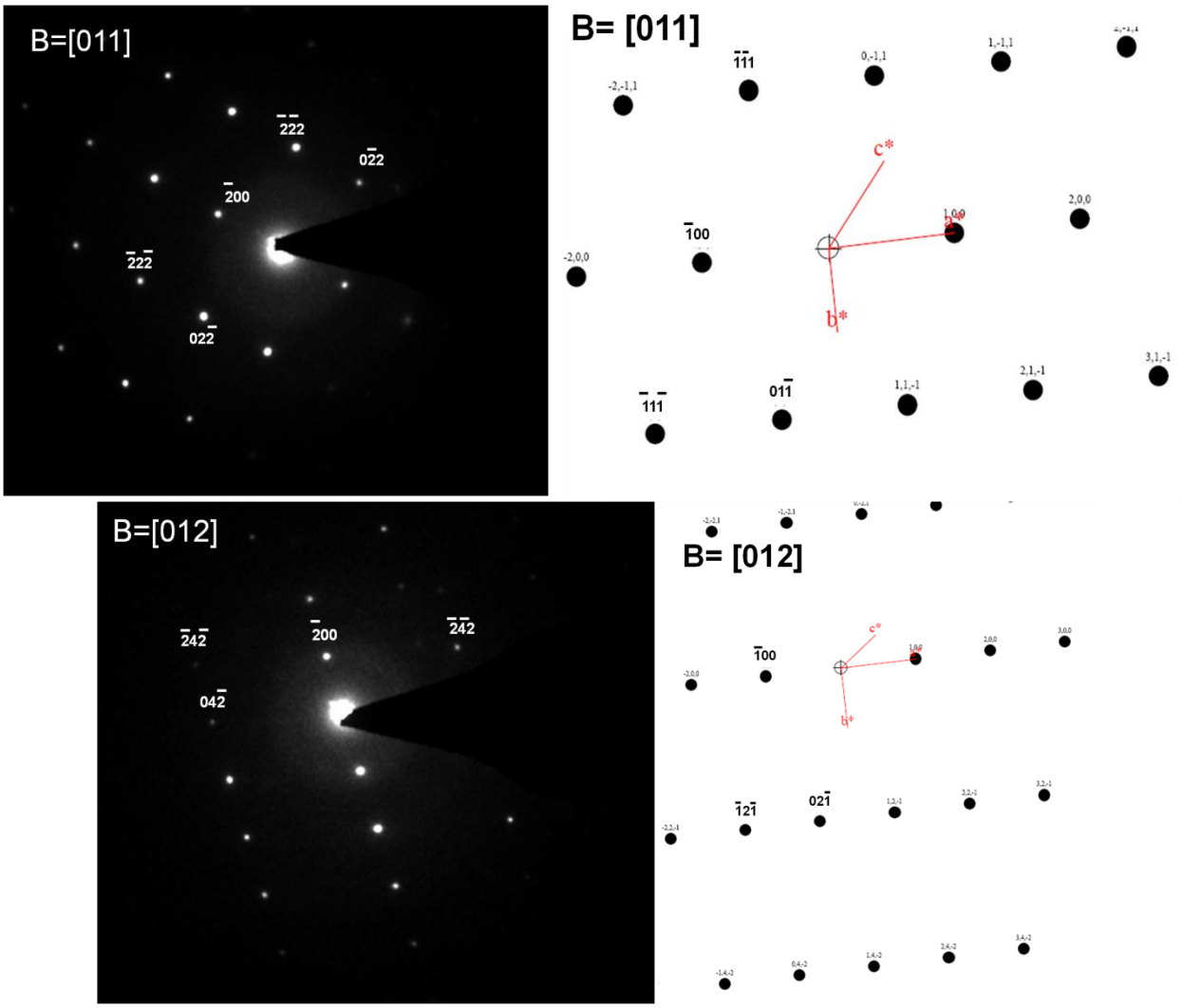

Comparison of angles between diffraction spots (planes) between TEM and XRD data for BFAS (3185) monoclinic structure

Zone-axis	011	012	$\alpha_{\text{zone 011}}$ / $\alpha_{\text{zone 012}}$	$\alpha'_{\text{zone 011}}$ / $\alpha'_{\text{zone 012}}$	$\beta_{\text{zone 011}}$ / $\beta_{\text{zone 012}}$	$\beta'_{\text{zone 011}}$ / $\beta'_{\text{zone 012}}$	$\gamma_{\text{zone 011}}$ / $\gamma_{\text{zone 012}}$	$\gamma'_{\text{zone 011}}$ / $\gamma'_{\text{zone 012}}$
Plane-1	0-11	02-1	43.67 / 22.81	41.88 / 21.44				
Plane-2	-1-11	-12-1			68.50 / 52.87	67.98 / 54.78		
Plane-3	-100	-100					39.59 / 76.15	41.35 / 78.71
Plane-4	-11-1	-1-21						

** α or α', β or β', γ or γ' are angles between Plane 1&2, Plane 2&3 and Plane 3&4, respectively.*

*** α, β, γ are angles from crystallographic software based on XRD data and α', β', γ' are angles from TEM analysis.*

Comparison of R-ratios between TEM and XRD data for BFAS (3185) monoclinic structure

Zone-axis	***011***	***012***	$R1/R2_{zone011}$/ $R1/R2_{zone\ 012}$	$R1/R2^*_{zone011}$/ $R1/R2^*_{zone\ 012}$	$R1/R3_{zone011}$/ $R1/R3_{zone012}$	$R1/R3^*_{zone011}$/ $R1/R3^*_{zone\ 012}$	$R1/R4_{zone011}$/ $R1/R4_{zone012}$	$R1/R4^*_{zone011}$/ $R1/R4^*_{zone\ 012}$
Plane-1	0-11	02-1	0.999 / 1.008	0.997 / 1.004	1.338 / 2.052	1.396 / 2.184	0.692 / 0.825	0.704 / 0.846
Plane-2	-1-11	-1-21						
Plane-3	-100	-100						
Plane-4	-11-1	-12-1						

** R1/R2 or R1/R2*, R1/R3 or R1/R3*, R1/R4 or R1/R4*, are R-ratios between Plane 1&2, Plane 1&3 and Plane 1&4, respectively.*

*** R1/R2, R1/R3, R1/R4 are ratios from crystallographic software based on XRD data and R1/R2*, R1/R3*, R1/R4* are ratios from TEM analysis.*

ATR-IR and Micro-Raman Spectroscopy

Infrared spectra were obtained using a Perkin Elmer FTIR (Spectrum BX model) spectrometer with a Miracle single bounce diamond ATR cell from PIKE Technologies. Spectra over the 4000–550 cm^{-1} range were obtained by the co-addition of 200 scans with a resolution of 4 cm^{-1} at the FWHM of the internal Polystyrene strongest C-H vibration.

Raman spectra were collected by an InVia Raman microscope from Renishaw in normal and Confocal mode. Laser excitation was provided by a polarized laser operating at 514 nm. The laser beam produced a spot size of approximately ≤ 5 µm in diameter using the 50x short distance objective. Averages of 10 scans were obtained from 4000 to 150 cm^{-1}. The energy resolution was 4 cm^{-1} at the full width half max (FWHM) of the internal Si reference peak. The scans were collected at 10 % of the laser output at the microscope exit to avoid radiation damage to the samples.

X-ray Photoelectron Spectroscopy

X-ray photoelectron spectroscopy (XPS) measurements were conducted in a Thermo Scientific K-Alpha, using an Al Kα X-ray source at 1486.6 eV with a pass energy of 20 eV. A 0.1 eV step size was used for all samples analyzed where the scale of the binding energy was calibrated against the Au ($4f_{7/2}$) peak at 84.0 eV and no effects due to charging or X-ray damage were observed and all measurements were conducted using a flood gun.

Structure Refinement

Crysfire

In the case of the pure BFS (3217), only lab based characterization techniques such as powder XRD (λ= 1.54Å), Raman and IR were employed and compared with the literature data. There was no need for synchrotron based analysis since the crystallographic nature of this material has already been published[2,4]. In the case of the arsenic containing BFS (3218), the arsenate (3185) and sulfate (3186) rich BFAS phases, high resolution synchrotron analysis was further conducted to determine their crystallographic structure using *ab-initio* methods.

For all structures, the crysfire suite was used to first fit the 33 resolvable peaks, accurately selected in the range 4–26 °2θ (λ= 0.4587Å) of our experimental pattern with a computed generated cell and extracting approximate initial lattice parameters and space groups to be used later in the structural refinements. The peaks of the arsenate containing Basic Ferric Sulfate 3218 (As-BFS) pattern were all successfully indexed in the space group *Immm* with lattice parameters *a* = 6.4197(6) Å, *b* = 7.1373(7) Å, *c* = 3.6709(3)

Å, while the ones of the 3185 (arsenate rich BFAS) pattern were all successfully indexed with lattice parameters *a* = 7.6066(15) Å, *b* = 7.2992(13) Å, *c* = 7.5423(13) Å in the possible space group $P2_1/c$. Likewise, the sulfate rich BFAS (3186) phase was found to have an overall $P2_1/c$ group with a large range of lattice parameters that was found to be a result of the fact this phase was found to be a mixture of two phases as will be shown later.

Endeavour

Endeavour[22] is a program for crystal structure solution from powder diffraction data using the "direct space" approach[26-28] It applies combined global optimization ("Simulated Annealing") for both the difference between the calculated and the measured diffraction pattern as well as the potential energy of the system. Size, shape and content of the unit cell must be known from experiment.

First, Endeavour calculations were run on the structure of the arsenate containing BFS (3218) compound. The diffraction pattern of this compound (which contains a small amount of As, replacing some of the S atoms) is very similar to the one described by Ventruti et al.[4] With regard to the small content of As replacing S in the compound/structure, it should be noted that the current version of Endeavour cannot handle partly occupied sites. Hence, it was not possible to model the exact S/As exchange in the structure. It was however possible to reproduce the main features of the structure (positions of Fe and some S atoms) if the As atoms were ignored. The structure of the arsenate containing BFS and BFS appear to be more or less equivalent to the Ventruti-structure[4], with the small difference that some S atoms are statistically replaced by As.

The structure of the arsenate rich BFAS(3185) (in which about two-thirds of the S atoms are "replaced" by As) was investigated using Endeavour. Because of Endeavour's current inability to use fractional occupation factors, a first calculation in which all S atoms were replaced by As was run. This assumption seemed to be as close to the "true" composition as possible, since in this case the amount of As in the compound was about twice as large as the amount of S (in contrast to As-BFS, where only very little As is present). Again, the corresponding calculation resulted in a structure related to the monoclinic polytype of the $FeOHSO_4$ OD-family[4]; however, the agreement was not as good as with the BFS compound mentioned before. The reason for this may be the relatively crude assumption to replace all S atoms by As. Notwithstanding this limitation there is nevertheless a strong indication from the Endeavour calculations that the basic structural features of the arsenate rich BFAS are at least similar to the ones of As-BFS and the Ventruti BFS structure. Because of the above site occupancy problem no further analysis with Endeavour in the case of the high sulfate (3186) containing BFAS was attempted and instead other refinement methods were employed via GSAS and DIFFaX+.

DIFFaX+ and GSAS

For structures that exhibited Order-Disorder behaviour most existing Rietveld codes, such as GSAS[23], cannot handle diffraction patterns affected by one-dimensional disorder exhibited by OD structures such as BFS. To overcome this issue, we made use of the program DIFFaX+, which has been specifically developed to study layered crystals showing stacking defects. This program combines the recursion algorithm of the DIFFaX–code[25] with the flexibility of a non-linear least-square routine to fit the simulated pattern to the observed one.[34-35] The recursion method allows to calculate diffraction effects in an one-dimensional disorder system taking into account a probability matrix for the occurrence of different layer sequences. The details of the algorithm and its theoretical basis are fully described by Treacy et al.[25]

In our case, a simple model of two identical layers, labeled L and L', with L' translated with respect to L, was considered to be sufficient to describe the whole OD family in structural simulations with DIFFaX+. The structure model of Johanson[2] was used to calculate the layer structure model. All ordered and disordered stacking sequences of equivalent layers can be described by just one parameter α ($=\alpha_{11}$), since $\alpha_{11} = \alpha_{22}$ and $\alpha_{11} + \alpha_{12} = 1$, describing the occurrence probability of layers sequence.

Refinement cycles were performed by DIFFaX+ for this model with the starting α value set to 0.5 (Figure S2). The refined parameters used were scale factor, zero-shift correction, lattice parameters, background, atomic positions, isotropic displacement parameters and stacking probabilities. The diffraction peaks were modeled with a pseudo-Voigt function allowing optimization of profile coefficients during refinement cycles.

The arsenate and sulfate rich BFAS phases were refined with GSAS as no Order-Disorder behavior was observed. In case where the structures such as the As-BFS exhibited Order-Disorder behavior[29-33], the X-ray diffraction pattern affected by the one dimensional order was refined with DIFFaX+.[25,34-35]

Li-ion cells fabrication, measurements and structures

The Li-Ion Coin Cell tested electrodes of our materials in this study were prepared and tested as outlined by Marks et al.[36] This method developed by the Dahn group was chosen as it gives high density, high capacity electrodes which have lower amounts of binder (similar to commercial electrodes) and carbon black material to provide sufficient adhesion and conductance. The reader is referenced to the article for detailed information.

To determine how the Li+ sites were placed along our structures (as in Figure 9-see manuscript) an examination of the framework of the structure has allowed to ascertain the occurrence of channels, along a axis, suitable for lithium insertion. best positions for Li into the framework along the a axis have been checked by means of the package Topos[37], that performs a topological analysis of structures and a search for channel systems and void positions

Section 2 : Supplementary Figures

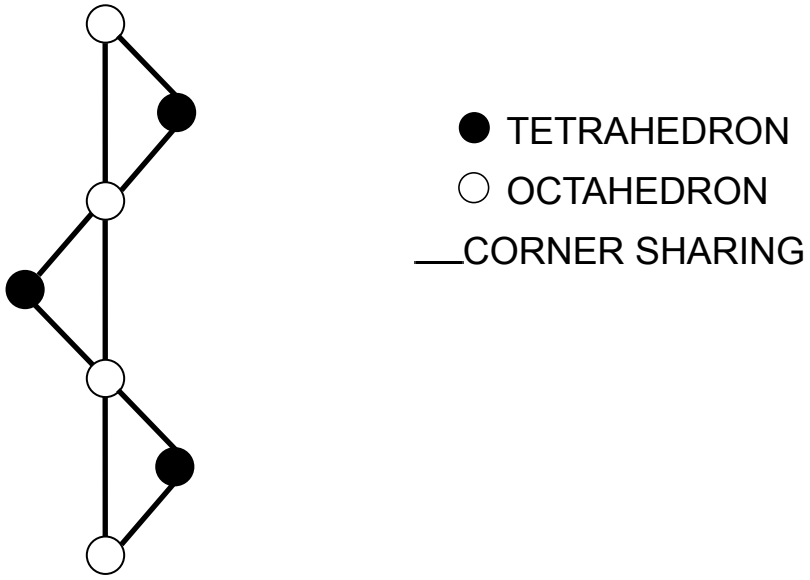

Figure S1. Graph of octahedral-tetrahedral chain present in the structure of butlerite ($FeOHSO_4 \bullet 2H_2O$), parabutlerite, uklonskovite ($NaMg(SO_4)F \bullet 2H_2O$) and basic ferric sulfate ($FeOHSO_4$).

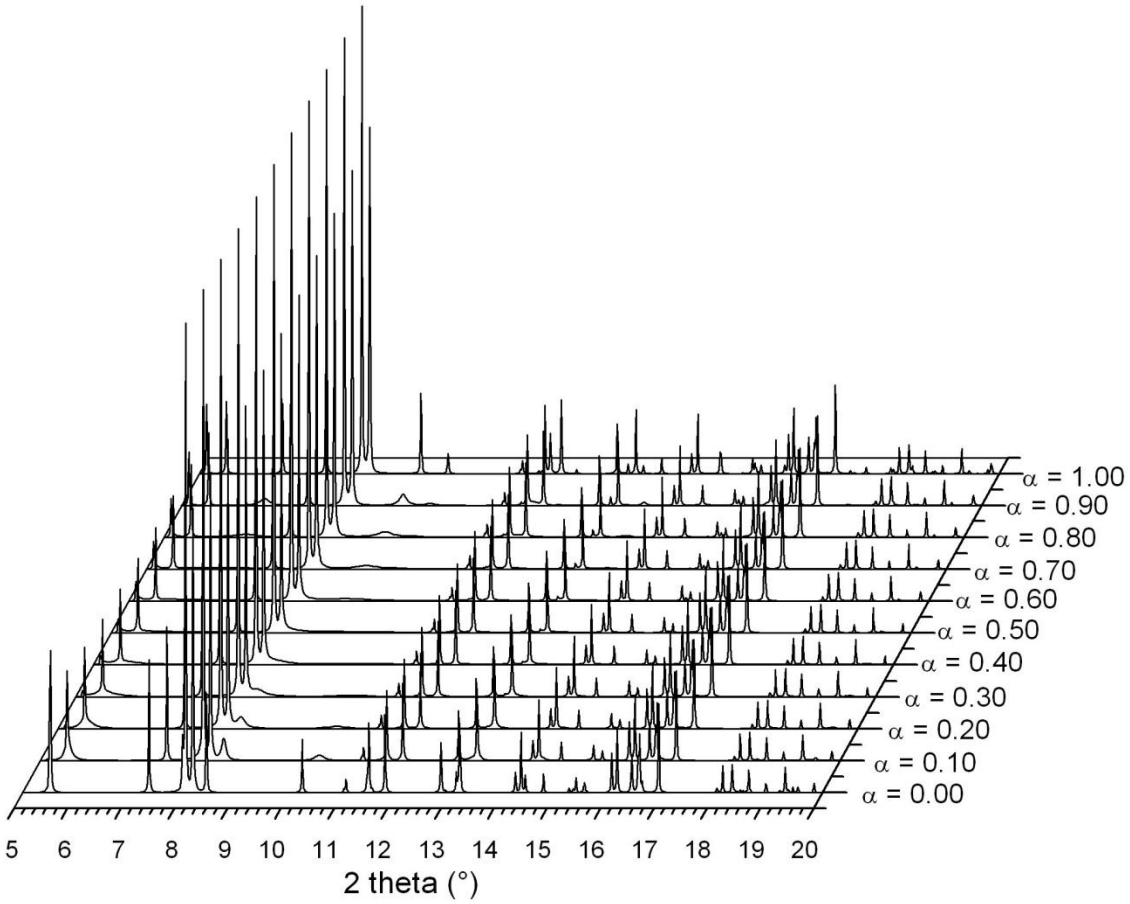

FIGURE S2. DIFFaX simulations of powder X-ray diffraction patterns as a function of the probability of monoclinic stacking, calculated for λ = 0.4587Å.

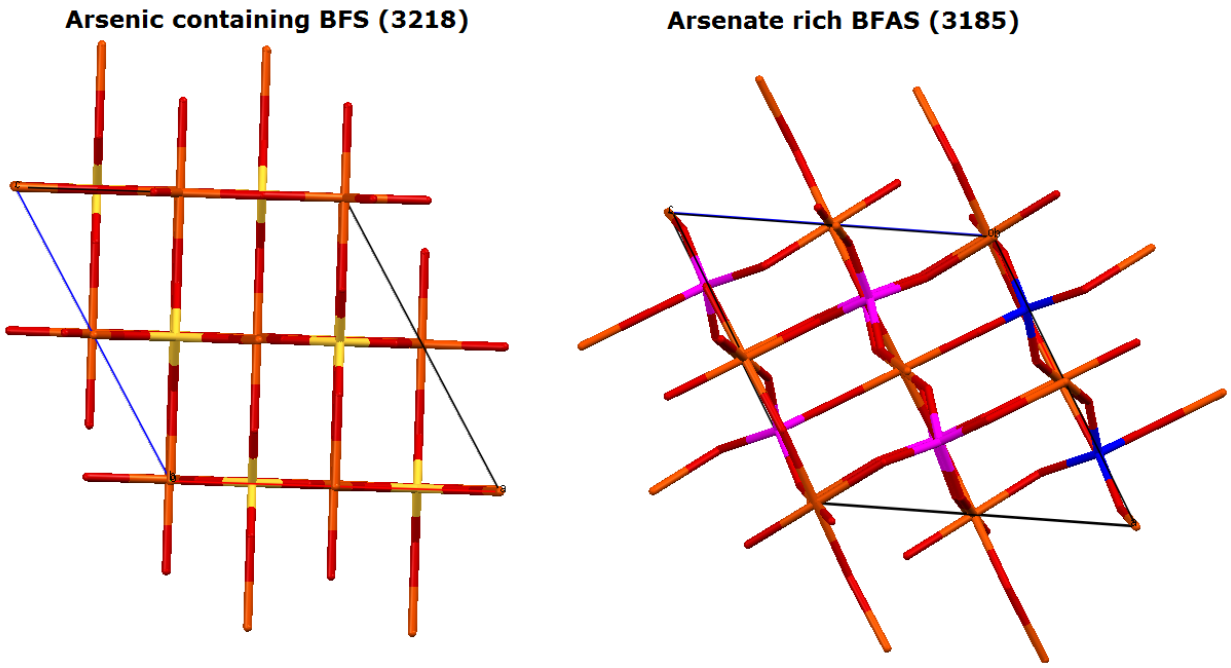

FIGURE S3. Structural comparison of the As-BFS and arsenate rich BFAS structure along the b-axis showing how the iron octahedra are distorted in the latter phase. It should be noted that for the arsenate rich BFAS phase, some TO_4 molecules were pictorially highlighted to indicate arsenate and sulfate replaced in the structure but as it may be observed from our crystallographic results no such site preference is observed for these molecules in the structure.

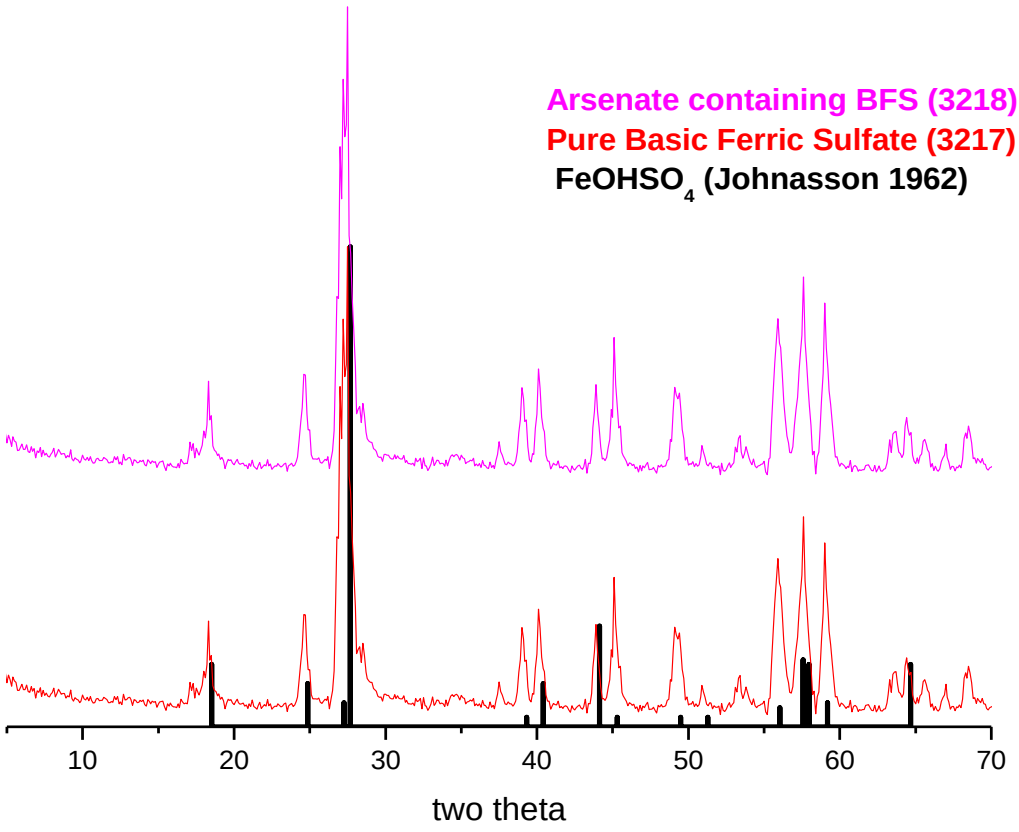

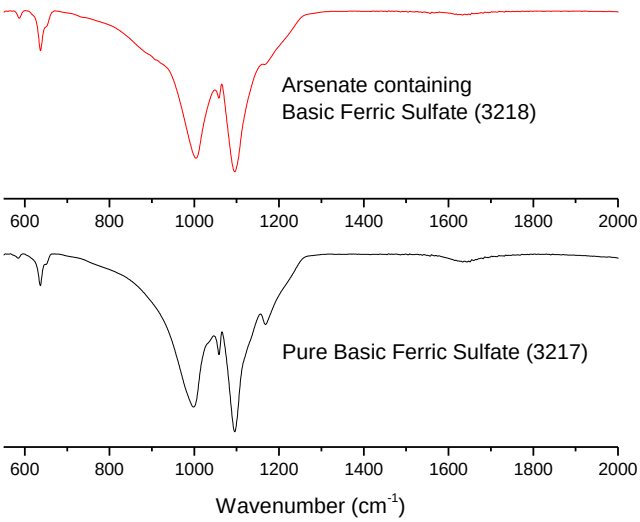

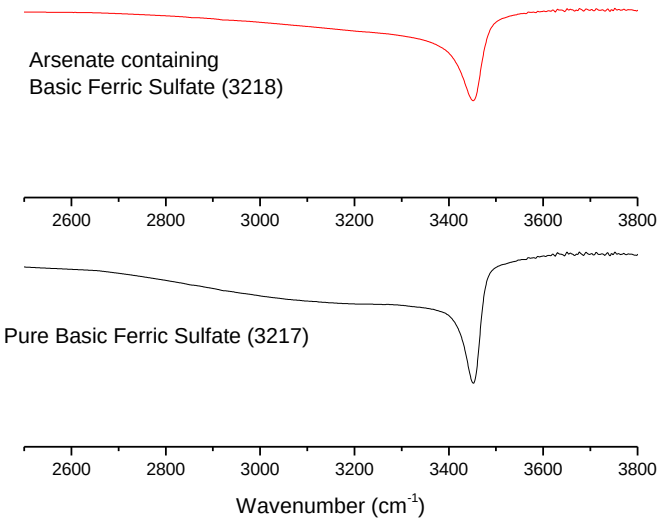

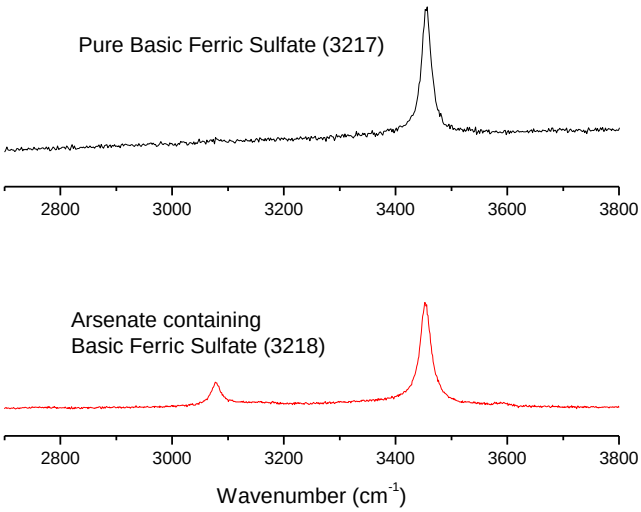

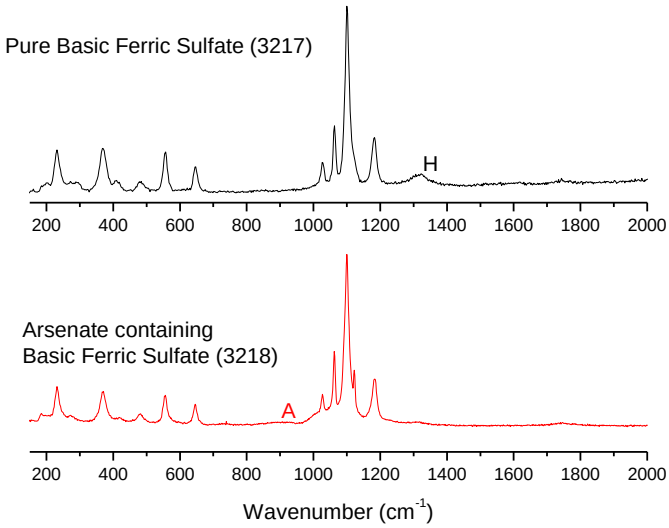

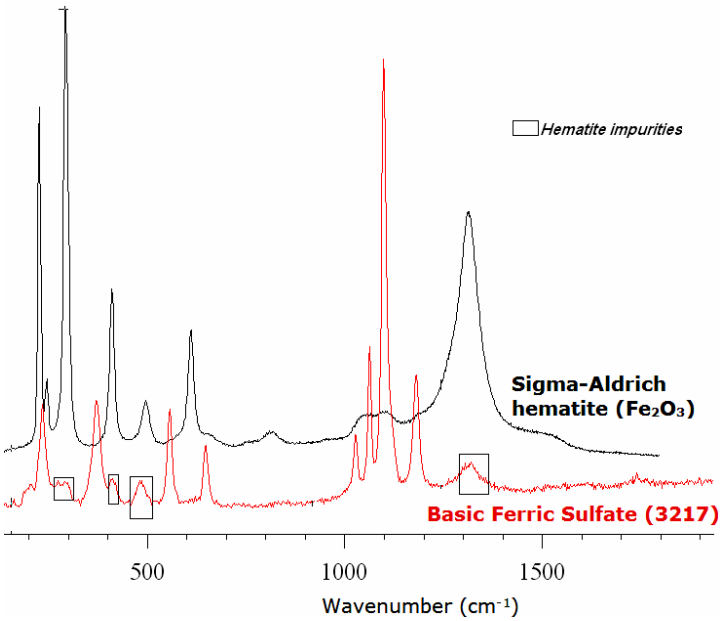

Figure S4. Lab based XRD (λ = 1.54Å), ATR-IR and Raman comparison of the pure BFS (3217) and the arsenate containing BFS (3218). The H and A symbols indicate the presence of hematite and arsenate. The last spectra shown the Raman spectra of the pure basic ferric sulfate (3217) in comparison to a reagent grade hematite standard to show some the contributions as in the lab based XRD, no real matches could be made with hematite.

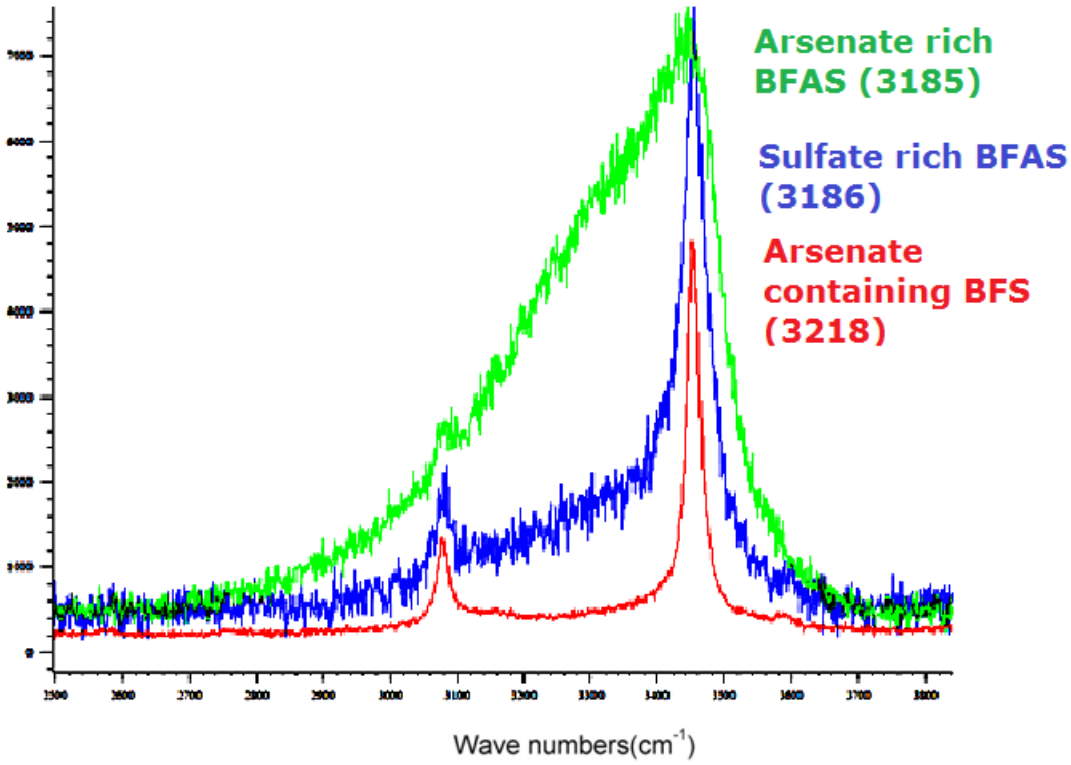

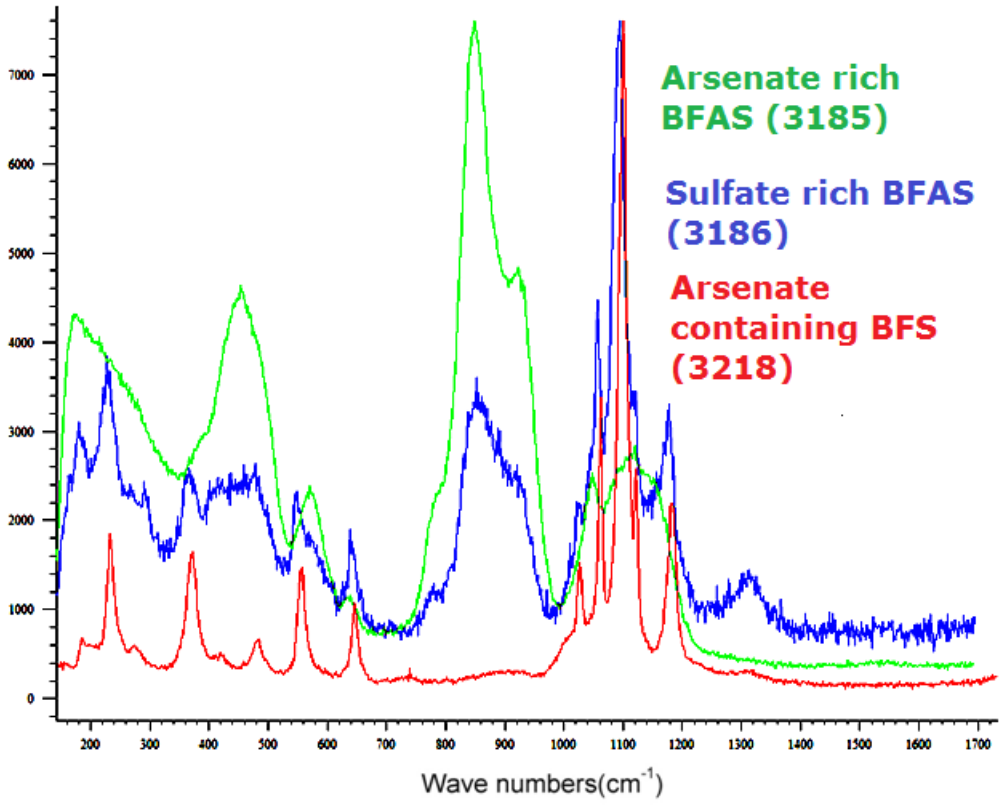

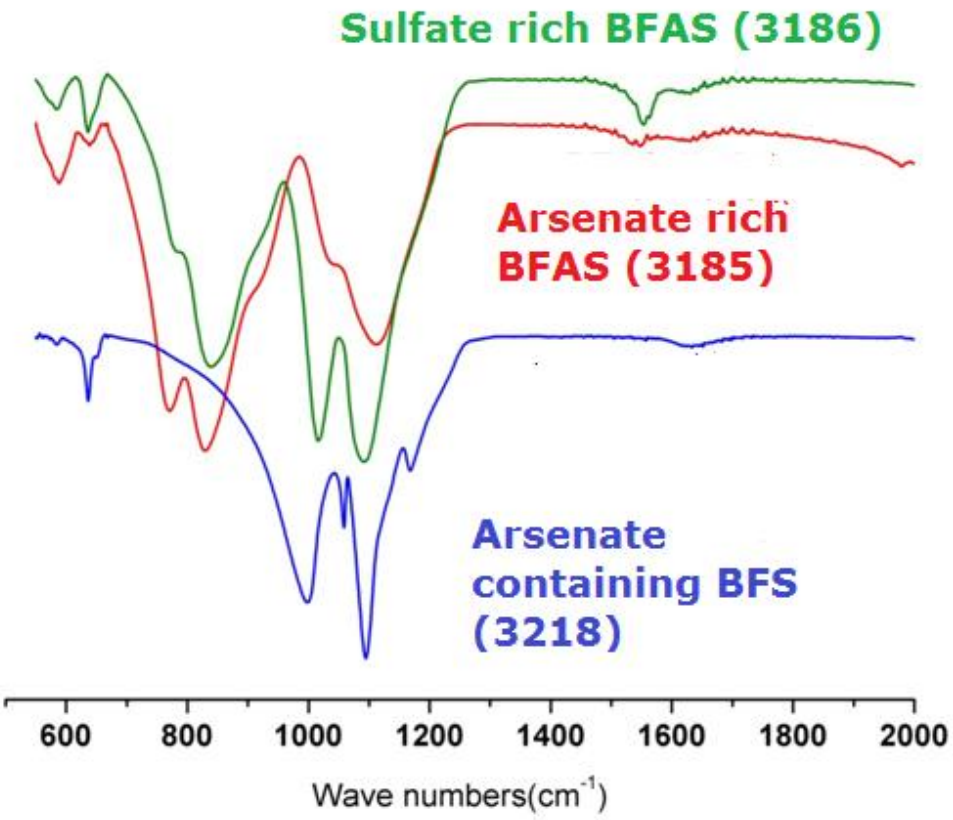

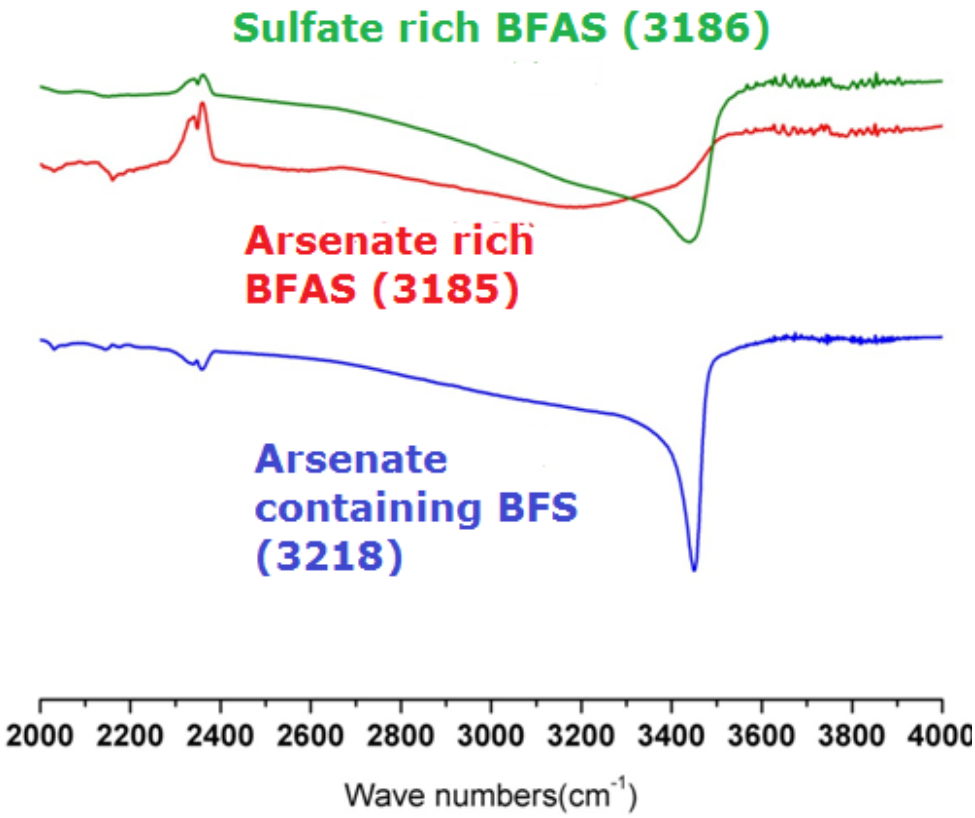

Figure S5. Raman and ATR-IR comparison of the arsenate containing BFS (3218), arsenate rich BFAS (3185) and sulfate rich BFAS (3186) .

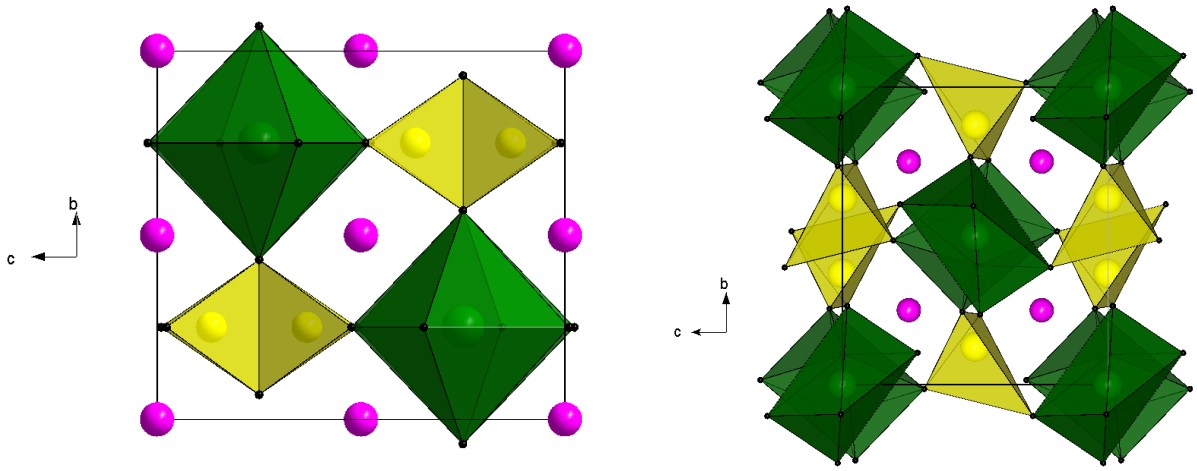

Figure S6. As-BFS (3218) and arsenate rich BFAS (3185) phases showing that the Li insertion occurs along *a-axis.*

Section 2 : Supplementary Tables

Table S1. Synthesis conditions and elemental solid composition (determined via ICP-OES) of ferric sulfate-arsenate phases used in this study.

Phase	Synthesis Conditions	Fe (w.t %)	AsO_4 (w.t. %)	SO_4 (w.t. %)	OH (w.t. %)	$H_2O^{\$}$ (w.t. %)
Basic Ferric Sulfate (3217)	0.53 M of Fe(III) @ 225 °C for 24	39[¥]	0	41	10	3
Arsenate containing Basic Ferric Sulfate (3218)	0.96 M of Fe(III), 0.08 M As (V) @ 225 °C for 5 hours	30	2	52	10	5
Arsenate rich Basic Ferric Arsenate Sulfate (3185)	0.30 M of Fe(III), 0.17 M As (V) @ 225 °C for 5 hours	30	46	17	10	10
Sulfate rich Basic Ferric Arsenate Sulfate (3186)	0.30 M of Fe(III), 0.08 M As (V) @ 225 °C for 5 hours	30	26	31	10	9

[¥] In this case the extra iron content was due to small amounts of hematite impurities (see below). Theoretically BFS has 33 w.t. % Fe, 56.8 w.t.% SO4 and 10w.t.% OH content.

[$] Determined from TGA analysis .[14]

Table S2a. Crystal data and Rietveld refinement parameters for the arsenate containing BFS (3218) phase.

Layer Symmetry	*Pnam*, (no. 62)
Layer parameters	a = 7.3415(2) Å
	b = 7.1365(2) Å
	c = 6.4197(2) Å
	V = 336.35(2) Å^3
	Z = 4
Transition probability	α=0.33 (4)
Rp(%)= 12.3	
Rwp(%)= 16.5	
Reduced χ^2 = 1.54	

Table S2b. Final atomic coordinates and isotropic displacements parameters (Å^2) for the arsenate containing BFS (3218) phase.

Atom	x/a	y/b	z/c	Occ.	U_{iso}
Fe	0.125(5)	0.250(2)	0.2500	1	0.002(1)
S	0.875(4)	0.867(1)	0.2500	0.96(1)	0.005(2)
As	0.875(4)	0.867(1)	0.2500	0.04(1)	0.005(2)
O1	0.375(7)	0.750(3)	0.067(2)	1	0.006(2)
O2	0.212(5)	0.510(3)	0.2500	1	0.006(2)
O3	0.953(6)	0.023(3)	0.7500	1	0.006(2)
O4	0.375(7)	0.154(2)	0.2500	1	0.006(2)

Table S2c. Selected bond distances (Å) and angles (°) for the arsenate containing BFS (3218) phase.

Fe-O1(*2)	2.035(13)			T-O1(*2)	1.441(17)
Fe-O2	1.962(30)			T-O2	1.484(40)
Fe-O3	2.031(30)			T-O3	1.487(26)
Fe-O4	1.959(54)				
Fe-O4	1.959(54)				
<Fe1-O>	1.997	<Fe2-O>	2.018	<T-O>	1.463
O1-Fe1-O1	180	O3-Fe2-O3	180	O1-T-O2	110.0(13)
O1-Fe1-O2	90.0(5)	O3-Fe2-O5	102.1(16)	O1-T-O3	107.8(11)
O1-Fe1-O3	90.0(5)	O3-Fe2-O4	91.3(12)	O1-T-O1	109.2(6)
O1-Fe1-O4	90.0(5)	O3-Fe2-O5	77.9(16)	O2-T-O3	111.9(13)
O1-Fe1-O4	90.0(9)	O5-Fe2-O5	180		
O2-Fe1-O3	96.1(10)	O5-Fe2-O4	89.9(32)		
O2-Fe1-O4	91.5(7)	O4-Fe2-O4	180		
O3-Fe1-O4	103.9(28)	O3-Fe2-O4	88.7(12)		
O3-Fe1-O4	83.9(10)	O5-Fe2-O4	90.1(32)		
O4-Fe1-O4	83.9(10)	O5-Fe2-O4	90.1(32)		

Table S3a. Crystal data and Rietveld refinement parameters for the arsenate rich BFAS (3185) phase.

Formula sum	$Fe(As_{0.84},S_{0.16})O_5H_{1.84}$
$Density_{calc}$	3.776 g/cm^3
Crystal system	monoclinic
Space group	$P2_1/c$, (no. 14)
Unit cell dimensions	a = 7.5980(5) Å
	b = 7.3063(5) Å
	c = 7.5580(8) Å
	β = 120.387(8) Å
Cell volume	361.93(6) Å^3
Z	4
Rp(%)= 15.1	
Rwp(%)= 22.3	
Reduced χ^2 = 2.14	

Table S3b. Atomic coordinates and isotropic displacements parameters ($Å^2$) parameters for the arsenate rich BFAS (3185) phase.

Atom	x/a	y/b	z/c	Occ.	U_{iso}
Fe	0.0000	0.0000	0.0000	1	0.007(1)
Fe	0.5000	0.5000	0.5000	1	0.007(1)
As	0.756(1)	0.617(1)	0.004(1)	0.84(4)	0.006(2)
S	0.756(1)	0.617(1)	0.004(1)	0.16(4)	0.006(2)
O1	0.156(4)	-0.046(5)	0.299(4)	1	0.010(2)
O2	0.051(3)	0.261(3)	-0.040(3)	1	0.010(2)
O3	0.432(3)	0.257(3)	0.032(4)	1	0.010(2)
O4	0.251(3)	-0.099(4)	0.003(3)	1	0.010(2)
O5	0.657(4)	0.481(4)	0.808(3)	1	0.010(2)

Table S3c. Selected bond distances (Å) and angles (°) for the arsenate rich BFAS (3185) phase.

Fe1-O1(x2)	1.98(3)	Fe2-O3(x2)	1.99(2)	T-O1	1.75(3)
Fe1-O2(x2)	2.00(2)	Fe2-O4(x2)	2.04(3)	T-O2	1.61(3)
Fe1-O4(x2)	2.03(3)	Fe2-O5(x2)	2.01(2)	T-O3	1.61(3)
				T-O5	1.62(3)
<Fe1-O>	2.00	<Fe2-O>	2.01	<T-O>	1.65
O1-Fe1-O1	180	O3-Fe2-O3	180	O1-T-O2	108.1(14)
O1-Fe1-O2	106.5(12)	O3-Fe2-O5	99.6(11)	O1-T-O3	117.2(16)
O1-Fe1-O4	84.8(11)	O3-Fe2-O4	88.1(11)	O1-T-O5	99.4(15)
O1-Fe1-O2	73.5(12)	O3-Fe2-O5	80.4(11)	O2-T-O3	111.5(14)
O2-Fe1-O2	180	O5-Fe2-O5	180	O2-T-O5	117.3(15)
O2-Fe1-O4	94.9(11)	O5-Fe2-O4	88.7(11)	O3-T-O5	103.5(15)
O4-Fe1-O4	180	O4-Fe2-O4	180		
O1-Fe1-O4	95.2(11)	O3-Fe2-O4	91.9(11)		
O2-Fe1-O4	85.1(11)	O5-Fe2-O4	91.3(11)		

Table S3d. Empirical bond-valence for the arsenate rich BFAS (3185) phase.

	O1	O2	O3	O4	O5	$\sum_c$
Fe1	0.55(x2)	0.52(x2)		0.49(x2)		3.12
Fe2			0.54(x2)	0.47(x2)	0.51(x2)	3.04
As,S	0.98	1.42	1.42		1.39	5.21
$\sum_a v$	1.53	1.94	1.96	0.96	1.90	

Table S4a. Crystal data and Rietveld refinement parameters for the sulfate rich BFAS (3186) phase.

Formula sum	$Fe(As_{0.75},S_{0.25})O_5H_{1.75}$
$Density_{calc}$	3.759 g/cm^3
Weight Fraction	0.533(2)
Crystal system	monoclinic
Space group	$P2_1/c$, (no. 14)
Unit cell dimensions	a = 7.5724(3) Å
	b = 7.2485(3) Å
	c = 7.5225(5) Å
	β = 120.287(5) Å
Cell volume	356.54(4) Å^3
Formula sum	$FeSO_5H$
$Density_{calc}$	3.325 g/cm^3
Weight Fraction	0.442(2)
Crystal system	monoclinic
Space group	$P2_1/c$, (no. 14)
Unit cell dimensions	a = 7.3526(2) Å

	b = 7.1394(2) Å
	c = 7.4041(5) Å
	β = 119.749(5) Å
Cell volume	337.44(3) Å^3
Formula sum	Fe_2O_3
Density$_{calc}$	5.239 g/cm^3
Weight Fraction	0.025(2)
Crystal system	trigonal
Space group	*R*-3*/c*, (no. 167)
Unit cell dimensions	a = 5.0293(6) Å
	c = 13.864(3) Å
	Cell volume 303.68(5) Å^3

Rp(%)= 10.7

Rwp(%)= 15.3

Reduced χ^2 = 1.69

Table S4b. Atomic coordinates and isotropic displacements parameters ($Å^2$) for the sulfate rich BFAS (3186) phase.

Atom	x/a	y/b	z/c	Occ.	U_{iso}
Fe	0.0000	0.0000	0.0000	1	0.008(1)
Fe	0.5000	0.5000	0.5000	1	0.008(1)
As	0.751(2)	0.616(2)	-0.001(1)	0.75(4)	0.007(2)
S	0.751(2)	0.616(2)	-0.001(1)	0.25(4)	0.007(2)
O1	0.157(5)	-0.041(5)	0.300(4)	1	0.009(2)
O2	0.058(4)	0.263(4)	-0.031(3)	1	0.009(2)
O3	0.443(4)	0.259(4)	0.046(3)	1	0.009(2)
O4	0.250(4)	-0.098(4)	-0.000(3)	1	0.009(2)
O5	0.656(4)	0.476(4)	0.807(3)	1	0.009(2)

Table S4c. Selected bond distances (Å) and angles (°) for the sulfate rich BFAS (3186) phase.

Fe1-O1(x2)	1.97(3)	Fe2-O3(x2)	2.00(3)	T-O1	1.73(3)
Fe1-O2(x2)	2.00(3)	Fe2-O4(x2)	2.02(3)	T-O2	1.60(3)
Fe1-O4(x2)	2.02(3)	Fe2-O5(x2)	2.00(2)	T-O3	1.61(3)
				T-O5	1.61(3)
<Fe1-O>	2.00	<Fe2-O>	2.01	<T-O>	1.64
O1-Fe1-O1	180	O3-Fe2-O3	180	O1-T-O2	107.0(16)
O1-Fe1-O2	103.7(12)	O3-Fe2-O5	103.2(10)	O1-T-O3	118.5(17)
O1-Fe1-O4	85.6(13)	O3-Fe2-O4	92.6(12)	O1-T-O5	99.8(16)
O1-Fe1-O2	76.3(12)	O3-Fe2-O5	76.8(10)	O2-T-O3	112.4(15)
O2-Fe1-O2	180	O5-Fe2-O5	180	O2-T-O5	116.1(16)
O2-Fe1-O4	94.3(12)	O5-Fe2-O4	87.7(10)	O3-T-O5	102.7(16)
O4-Fe1-O4	180	O4-Fe2-O4	180		
O1-Fe1-O4	94.4(13)	O3-Fe2-O4	87.1(10)		
O2-Fe1-O4	85.7(12)	O5-Fe2-O4	92.3(10)		

Table S4d. Atomic coordinates and isotropic displacements parameters ($Å^2$) for the sulfate rich BFAS (3186) phase.

Atom	x/a	y/b	z/c	Occ.	U_{iso}
Fe	0.0000	0.0000	0.0000	1	0.004(1)
Fe	0.5000	0.5000	0.5000	1	0.004(1)
S	0.7528(10)	0.6099(11)	0.0020(9)	1	0.018(2)
O1	0.1574(35)	-0.0160(38)	0.3125(29)	1	0.017(2)
O2	0.0800(29)	0.2683(30)	-0.0050(24)	1	0.017(2)
O3	0.4144(29)	0.2668(30)	0.0030(23)	1	0.017(2)
O4	0.250(3)	-0.107(4)	0.000(3)	1	0.017(2)
O5	0.6608(30)	0.4888(35)	0.8128(30)	1	0.017(2)

Table S4e. Selected bond distances (Å) and angles (°) for the sulfate rich BFAS (3186) phase.

Fe1-O1(x2)	2.02(2)	Fe2-O3(x2)	2.01(2)	T-O1	1.49(2)
Fe1-O2(x2)	2.01(2)	Fe2-O4(x2)	1.99(3)	T-O2	1.50(2)
Fe1-O4(x2)	1.99(3)	Fe2-O5(x2)	2.01(2)	T-O3	1.49(2)
				T-O5	1.49(2)
<Fe1-O>	2.01	<Fe2-O>	2.00	<T-O>	1.49
O1-Fe1-O1	180	O3-Fe2-O3	180	O1-T-O2	110.5(14)
O1-Fe1-O2	94.0(9)	O3-Fe2-O5	92.4(9)	O1-T-O3	111.3(14)
O1-Fe1-O4	88.6(9)	O3-Fe2-O4	93.9(10)	O1-T-O5	107.5(15)
O1-Fe1-O2	86.0(9)	O3-Fe2-O5	87.6(9)	O2-T-O3	108.4(13)
O2-Fe1-O2	180	O5-Fe2-O5	180	O2-T-O5	109.7(12)
O2-Fe1-O4	95.0(10)	O5-Fe2-O4	88.3(9)	O3-T-O5	109.5(12)
O4-Fe1-O4	180	O4-Fe2-O4	180		
O1-Fe1-O4	91.4(9)	O3-Fe2-O4	86.1(10)		
O2-Fe1-O4	85.0(10)	O5-Fe2-O4	91.7(9)		

Table S5. Factor group distribution of the internal modes of XO_4 (X=S or As) molecules in the MDO1 (*Pnma*=D_{2h}) structure in BFS and As-BFS.

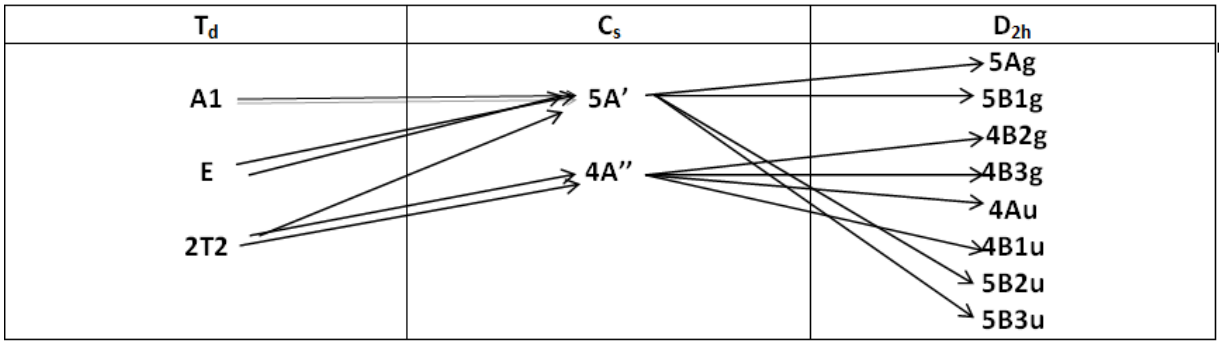

Table S6. Factor group distribution of the internal modes of XO_4 (X=S or As) molecules in the MDO2 ($P2_1/c$=C_{2h}) structure in BFS and As-BFS.

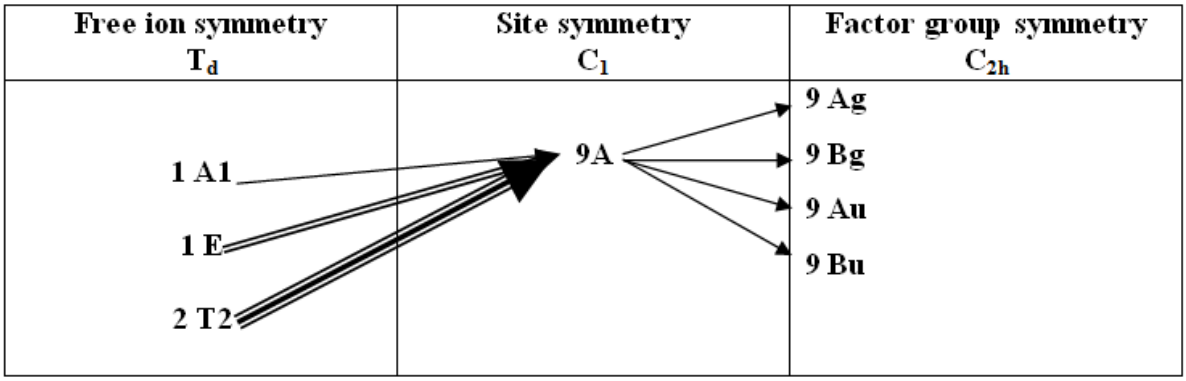

Table S7. Factor group distribution of the internal modes of XO_4 (X=S or As) molecules for the overall OD (*Immm*=D_{2h}) structure that occurs in BFS[6,8] and As-BFS (3218).

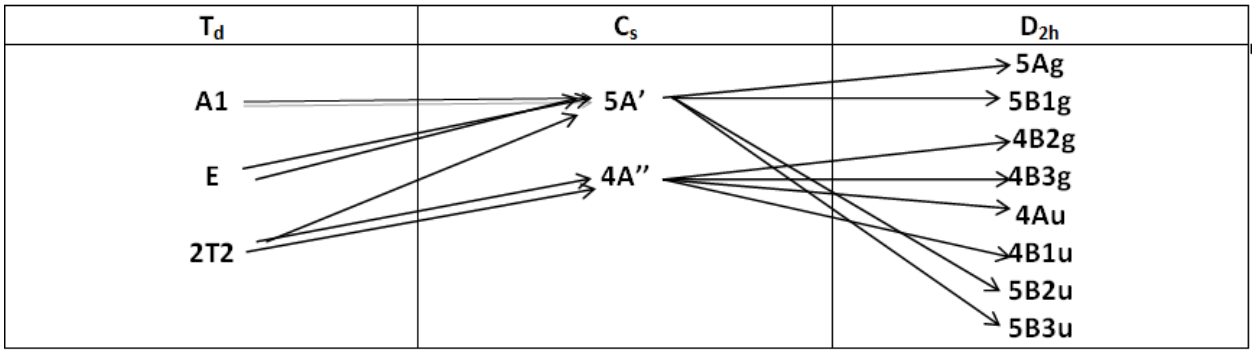

Table S8. Proposed vibrational band assignments for As-BFS (3218), arsenate rich BFAS (3185) and sulfate rich BFAS (3186). For the pure BFS (3217) similar values[≠] and assignments as those in Powers et al.[39] were obtained and as such are not repeated in this table.

As-BFS (3218)			Sulfate rich BFAS (3186)			Arsenate rich BFAS (3185)		
Raman	**IR**	**Assign**	**Raman**	**IR**	**Assign**	**Raman**	**IR**	**Assign**
3587	3452	OH str	3456	3450	OH str	3444	3414	OH str
3453				3179			3171	
3077	-	H_2O str	3084	-	H_2O str	-	1630	H_2O bend
-	1632	H_2O bend	-	1632	H_2O bend	1159	1112	$V_3(SO_4)$
1183	1168		1179	1105	$V_3(SO_4)$	1123	-	
1122	1095	$V_3(SO_4)$	1060	1058		1050	1038	$V_1(SO_4)$
1062	1058		1028	1016	$V_1(SO_4)$	925	918	$V_3(AsO_4)$
1100	-		927	919	$V_3(AsO_4)$	850	829	
914	-	$V_3(AsO_4)$	850	848		789	771	$V_1(AsO_4)$
1026	999	$V_1(SO_4)$	782	779	$V_1(AsO_4)$	639	638	$V_4(SO_4)$
-	-		645	653	$V_4(SO_4)$			
-	-		-	638		576	587	$FeOH_2$ str
-	-		-	-		456	-	$V_4(AsO_4)$ /
645	651	$V_4(SO_4)$	551	587	$FeOH_2$ str	-		$V_2(SO_4)$
556	632		476	-	$V_4(AsO_4)$ /	-		
-	584	$FeOH_2$ str	417	-	$V_2(SO_4)$	178		External and
-			-	-				Lattice
480		$V_2(SO_4)$	-	-				Modes
418			-	-				
			368	-	External and			
370		External	-		Lattice			
231		and Lattice	-		Modes			
-		Modes	-					
-								
-								
-								

[≠]For our pure BFS (3217) Raman bands were observed at 3455, 1322, 1184, 1100, 1063, 1026, 645, 557, 481, 410, 370, and 231 cm^{-1}. IR bands were observed at 3453, 1169, 1096, 998, 652, 637 and 585 cm^{-1}.

Table S9. Hydrogen bond lengths (Å) calculated using the regression functions $\nu = 3592-(304*10^9)\exp(-d_{O\cdots O}/0.1321)$ and $\nu = 3632-(1.79*10^6)\exp(-d_{H\cdots O}/0.1321)$ from Libowitzky[40] using the ATR-IR and Raman hydroxyl stretching frequencies observed in this study.

BFS (3217)		**As-BFS (3218)**		**Arsenate rich-BFAS (3185)**		**Sulfate rich-BFAS (3186)**	
H···A[1]	**D···A[2]**	**H···A**	**D···A**	**H···A**	**D···A**	**H···A**	**D···A**
1.21 Å ($3453\ cm^{-1}$) IR	2.84Å ($3453\ cm^{-1}$) IR	1.21 Å ($3452\ cm^{-1}$) IR	2.83Å ($3452\ cm^{-1}$) IR	1.19 Å ($3414\ cm^{-1}$) IR	2.80Å ($3414\ cm^{-1}$) IR	1.21 Å ($3450\ cm^{-1}$) IR	2.83Å ($3450\ cm^{-1}$) IR
				1.09 Å ($3171\ cm^{-1}$) IR	2.73 Å ($3171\ cm^{-1}$) IR	1.09 Å ($3179\ cm^{-1}$) IR	2.74 Å ($3179\ cm^{-1}$) IR
1.21 Å ($3455 cm^{-1}$) Raman	2.84 Å ($3455\ cm^{-1}$) Raman	1.40 Å ($3587\ cm^{-1}$) Raman	3.28Å ($3587\ cm^{-1}$) Raman	1.21 Å ($3444\ cm^{-1}$) Raman	2.83Å ($3444\ cm^{-1}$) Raman	1.22 Å ($3456\ cm^{-1}$) Raman	2.84Å ($3456\ cm^{-1}$) Raman
		1.21Å ($3453\ cm^{-1}$) Raman	2.84 Å ($3453\ cm^{-1}$) Raman			1.06 Å ($3084\ cm^{-1}$) Raman	2.64 Å ($3084\ cm^{-1}$) Raman
		1.06Å ($3077\ cm^{-1}$) Raman	2.64Å ($3077\ cm^{-1}$) Raman				

[#] The band maximum was used to calculate the H-bond distances as no other clear features like the shoulder observed in the natural minerals were present.

[1] H···A represents the distance in the H-bond between M-OH/H_2O and O-T units

[2] D···A represents the distance in the H-bond between M-OH/H_2O and O-T units

*In these phases, the D-H (M-OH/OH_2) units are the H-bond donors and the A groups (TO_4 where T = S or As) are the acceptors upon H-bonding complexation (D-H···A) in the molecular lattice.

Table S10. XPS As 3d fitting and spin-orbit values of the various materials and standards used in this study (± 0.1 eV).

Sample	A	B	Δ(S-O)
Scorodite	46.00	45.19	0.81
As_2O_3	45.33	44.58	0.75
BFAS (3185)	45.22	44.69	0.53
BFAS (3186)	45.23	44.96	0.27
As-BFS (3218)	45.49	45.4	0.10

Table S11. XPS O 1s fitting of the various materials and standards used in this study (± 0.1 eV).

Sample	A (H_2O)	B(OH^-)	C (O^{-2})
BFAS (3185)	533.27	531.43	530.66
BFAS (3186)	533.18	531.66	530.40
As-BFS (3218)	533.50	531.84	530.10

Table S12. XPS S 2p fitting and spin-orbit (S-O) values of the various materials and standards used in this study (± 0.1 eV).

Sample	A	B	Δ(S-O)
BFAS (3185)	170.07	168.77	1.30
BFAS (3186)	169.92	168.69	1.23
As-BFS (3218)	170.09	168.84	1.25

Section 4: References

[1] T. C. Cheng, G. P. Demopoulos, *Ind. Eng. Chem. Res*. 2004, **43**, 6299-6308.

[2] G. Johansson, *Acta Chem. Scand*. 1962, **16**, 1234-1244.

[3] M. Anji Reddy, V. Pralong, V. Caignaert, U.V. Varadaraju, B. Raveau, *Electrochem. Commun*. 2009, **11**, 1807–1810.

[4] G. Ventruti, F. Scordari, E. Schingaro, A. Gualtieri, C. Meneghini, *Am. Mineral*. 2005, **90**, 679-686.

[5] C. A. Fleming, *Miner. Metall. Process.* 2010, **27**, 81-88.

[6] L. Becze, M. A. Gomez, J. F. Le Berre, B. Pierre, G. P. Demopoulos, *Can. Metall. Q.* 2009, **48**, 99-108.

[7] R. Berezowsky, T. Xue, M. Collins, M. Makwana, I. Barton-Jones, M. Southgate, J Maclean, *JOM*, 1999, **51**, 36-40.

[8] J. Xu, N. Gao, Y. Tang, Y. Deng, M. Sui, *J. Environ. Sci*., 2010, **22**, 1807–1813.

[9] P. B. Moore, *Neues Jahrb. Mineral. Monatsh.* 1970, 163–173.

[10]. F. C. Hawthorne, S. V. Krivovichev, P. C. Burns, *Rev. Mineral. Geochem*. 2000, **40**, 1–112.

[11] P. M. Swash, A. J. Monhemius, “Hydrothermal precipitation from aqueous solutions containing iron (III), arsenate and sulfate”, *In Hydrometallurgy ’94*, Chapman & Hall (New York, N.Y.) 1994, pp.177-190

[12] N. Papassiopi, E. Virkov, V. Nenov, A. Kontopoulos, L. Molnhr, *Hydrometallurgy*, 1996, **41**, 243-253.

[13] J. E. Dutrizac, J. L. Jambor, J. L., *Hydrometallurgy*, 2007, **86**, 147-163.

[14] M. A. Gomez, L. Becze, J. N. Cutler, G. P. Demopoulos, *Hydrometallurgy,* 2011, **107**, 74-90.

[15] M. A. Gomez, H. Assaaoudi, L. Becze, J. N Cutler, G. P. Demopoulos, *J. Raman Spectrosc*. 2010, **41**, 212-221.

[16] R. C. M. Mambote, M. A. Reuter, A. van Sandwijk, P. Krijgsman, *Miner. Eng*. 2001, **14**, 391-403.

[17] H. McCreadie, D. W. Blowes, C. J. Ptacek, J. L. Jambor, *Environ. Sci. Technol*. 2000, **34**, 3159–3166.

[18] M. A. Gomez, L. Becze, M. Celikin, G. P. Demopoulos, *J. Colloid Interface Sci*. 2011, **360,** 508-518.

[19] M. A. Gomez, J. F. Le Berre, H. Assaaoudi, G. P. Demopoulos, *J. Raman Spectrosc.* 2011, **42**, 62-71.

[20] R. L. Frost, Y. Xi, K. Tan, J. Miller, S. J. Palmer, *Spectrochimica Acta Part A*, 2012, **85**, 173-175.

[21] J. Wang, B. H. Toby, P. L. Lee, L. Ribaud, S. M. Anyao, C. Kurtz, M. Ramanathan , R. B. Von Dreele, M. A. Beno, *Rev. Sci. Instrum*. 2008, **79**, 085105-1–085105-7.

[22] H. Putz, J.C. Schoen, M. Jansen, *J. Appl. Cryst*. 1999, **32**, 864-870.

[23] A. C. Larson, R. B. V. Dreele, *Los Alamos National Laboratory Report LAUR*, 2000, pp. 86– 748

[24] B. H. J. Toby, *Appl. Crystallogr.* 2001, **34***,* 210– 213.

[25] M. M. J. Treacy, J. M. Newsam, M. W. Deem, *Proc. R. Soc. London, Ser. A*, 1991, **433,** 499–520.

[26] Y. G. Andreev, G. S. MacGlashan, P. G. Bruce, *Phys. Rev. B*, 1997, **55,** 12011 - 12017.

[27] K. Shankland, W. I. F. David, T. Csoka*, Z. Kristallogr*. 1997, **212**, 550-552.

[28] K. D. M. Harris, R. L. Johnston, B. M. Kariuki, *Acta Cryst. A*, 1998, **54**, 632-645.

[29] K. Dornberger-Schiff, *Abh dtsch Akad Wiss Berlin, Kl f Chem*. 1964, **3**, 1–107.

[30] K. Dornberger-Schiff, K. Fichtner, *Kristall und Technik*., 1972, **7**, 1035–1056.

[31] S. Merlino, *Periodico di Mineralogia*, 1990, **59**, 69–92.

[32] E. Michalsky, *Acta Crystallographica*, 1988, **A44**, 640–649.

[33] E. Michalsky, S. Kaczmarek, M. Demianiuk, *Acta Crystallographica*, 1988, **A44**, 650–657.

[34] A. F. Gualtieri, *Eur. J. Mineral.*, 1999, **11**, 521–532.

[35]. A. Viani, A. F. Gualtieri, G. Artioli, *Am. Mineral.* 2002, **87**, 966–975.

[36] T. Marks, S. Trussler, A. J. Smith, D. Xiong, J. R. Dahn, *J. Electrochem. Soc*. 2011, **158**, A51–A57.

[37] V. A. Blatov and A. P. Shevchenko, *Acta Crystallographica*, 2003, **A59**, 34–44.

.